J Mater Sci: Mater Electron (2015) 26:1959–1968
DOI 10.1007/s10854-014-2635-2

Synthesis, dielectric properties of $Bi_{2/3}Cu_3Ti_4O_{12}$ ceramics by the sol–gel method

Zhao Yang · Pengfei Liang · Longhai Yang · Pinging Shi · Xiaolian Chao · Zupei Yang

Received: 30 September 2014 / Accepted: 16 December 2014 / Published online: 1 January 2015

Abstract $Bi_{2/3}Cu_3Ti_4O_{12}$ ceramics were synthesized by the sol–gel method. The optimum parameters for the synthesis of precursor powders were as follows: the Ti concentration was 0.62 mol/L, the aging time of the sol was 16 h and the reaction temperature was 40 °C. When calcined at 800 °C and sintered at 1,000 °C, $Bi_{2/3}Cu_3Ti_4O_{12}$ ceramics with the highest density and fine-grained microstructure were obtained. The resultant ceramics showed outstanding dielectric properties with a dielectric constant (ε') of $\sim 1.2 \times 10^4$ measured at 1 kHz. The dielectric constant was much higher than that of the ceramics with same composition prepared by the solid-state reaction ($\sim 0.30 \times 10^4$ at 1 kHz). A unique phenomenon was observed in the temperature dependence of dielectric constant. Dielectric relaxation I occurred at $\sim$200 °C was due to the Maxwell–Wagner relaxation. Whereas an additional dielectric relaxation II was observed at $\sim$300 °C only for the sample prepared by the sol–gel method, which was ascribed to the distribution state transition for oxygen vacancies.

1 Introduction

Materials with high dielectric permittivity, low dielectric loss, and good temperature stability are essential to the miniaturization of many capacitance-based electronic devices such as capacitors, resonators, and filters. $CaCu_3Ti_4O_{12}$ (CCTO) has attracted a significant amount of attention because of its colossal dielectric permittivity (10^4) and insignificant temperature dependence over a wide temperature range from 100 to 500 K [1]. For a considerably long time period, CCTO was believed as a peculiar material among the large number of perovskite-related oxides that can be generally described with a compositional formula of $ACu_3Ti_4O_{12}$ [1–3]. Interestingly, several other oxides of $ACu_3Ti_4O_{12}$ have been confirmed very recently in experiments to indeed exhibit giant-ε' behaviors [4–7]. $Bi_{2/3}Cu_3Ti_4O_{12}$ (BCTO) is one of the few members that have been presently confirmed isostructurally CCTO-like oxides. However, limited literatures reported the BCTO ceramics prepared by the solid-state reaction [6, 8], and the dielectric constant of the ceramics is relatively low for practical applications. Consequently, the work aims to enhance the dielectric constant of BCTO ceramics.

As one of the wet chemical methods, the sol–gel method is based on synthesis from a solution. This affords a homogeneous mixing of the metal ions at an atomic scale, thus leading to finer powders endow ceramics with good microstructure and excellent dielectric properties. In recent years, CCTO [9], NBCTO [10] and NLCTO [11] ceramics with improved dielectric properties have been successfully synthesized by the sol–gel method. Currently, there are scarce reports on BCTO ceramics prepared by the sol–gel method. This may be due to the hydrolysis of compounds containing bismuth, which makes the composition of the resultant ceramics uncontrollable.

In the present work, BCTO ceramics were successfully prepared by the sol–gel method. The impact of coagulating conditions (Ti concentration, reaction temperature, aging time), calcining temperature and sintering temperature on

Z. Yang · P. Liang · L. Yang · P. Shi · X. Chao · Z. Yang (✉)
Key Laboratory of Macromolecular Science of Shaanxi Province, School of Materials Science and Engineering, Shaanxi Normal University, Xi'an 710062, Shaanxi, People's Republic of China
e-mail: yangzp@snnu.edu.cn

X. Chao
e-mail: chaoxl@snnu.edu.cn

the phase structure, microstructure, dielectric properties of the ceramics were investigated in detail. The impedance spectroscopy was used to explore the origin of giant dielectric constants. The temperature dependence of dielectric constant was studied as well. In addition, the differences on dielectric properties between ceramics prepared by the sol–gel method and by solid-state reaction were compared.

2 Experimental procedure

The $Bi_{2/3}Cu_3Ti_4O_{12}$ (BCTO) samples were prepared by a sol–gel method. Bismuth nitrate ($Bi(NO_3)_3{\cdot}5H_2O$, 99 %), copper nitrate ($Cu(NO_3)_2{\cdot}3H_2O$, 99 %) and tetrabutyl titanate ($Ti(OC_4H_9)_4$, 98 %) were weighed in an appropriate molar ratio as starting materials. $Cu(NO_3)_2{\cdot}3H_2O$, $Bi(NO_3)_3{\cdot}5H_2O$ were dissolved in the buffer mixed solution of ethanol and deionized water (C_2H_5OH:H_2O = 1:1) which was solution 1, particularly, $Bi(NO_3)_3{\cdot}5H_2O$ was dissolved in 2 mol/L HNO_3 due to its hydrolyzation. $Ti(OC_4H_9)_4$, glacial acetic solution (CH_3COOH) and ethanol were mixed to obtain solution 2. The two solutions were constantly stirring under vigorous stirring by a magnetic stirrer, the color of the solution turned light blue followed by a vigorous stirring. The mixed solution was held in a water bath at 40 °C until it turned completely to a gel. The gel was then aged for 16 h. After that, the gel was dried at 120 °C, and then was calcined at 800 °C for 10 h. The obtained powders were ground with polyvinyl alcohol solution. Then the obtained powders were ground with polyvinyl alcohol solution and compacted into pellets with 15 mm in diameter and about 1.0 mm in thickness. These compacts were fired at up to 1,000 °C for 7.5 h with a ramp rate of 2 °C min^{-1}.

For comparison, BCTO ceramics were also prepared by the solid-state method. The stoichiometric amounts of highly pure Bi_2O_3 (99.0 %), CuO (99 %), TiO_2 (99.99 %) were mixed and ball-milled in ethanol for 10 h. Subsequently, the slurry were dried and calcined at 800 °C for 10 h in air. The obtained powders were ground with PVA and compacted into pellets with the same diameter and thickness. These pellets were also fired with the same procedure as the pellets obtained by the sol–gel method.

The crystal structures of ceramics with surface polishing were investigated by X-ray diffraction (XRD, D/max-2550/PC, Rigaku, Japan) technique using Cu Kα radiation. Microstructures were observed with the scanning electron microscopy (SEM, Quanta 200, Philips, Netherlands). For the purpose of measuring the electric properties, both sides of the samples were coated by silver paste and fired at 840 °C to form electrodes. Dielectric dispersion and complex impedance were measured at room temperature using an Agilent 4294A impedance analyzer within a frequency range of 40 Hz to 110 MHz. Temperature dependence of the dielectric constant was investigated by the LCR meter (Agilent, E4980A).

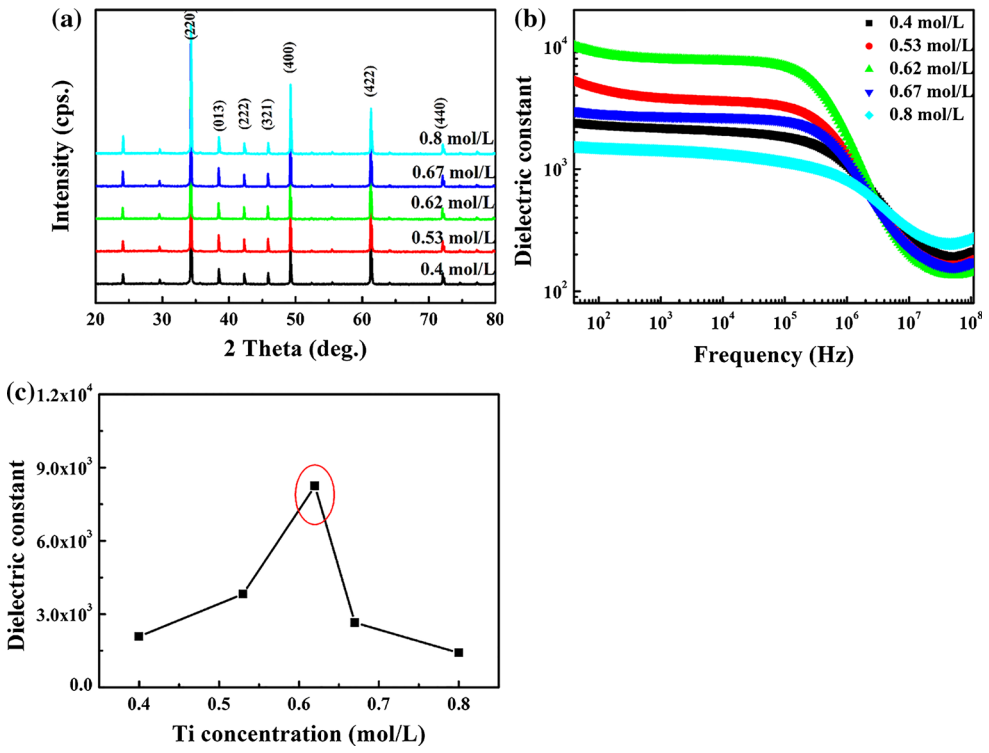

Fig. 1 **a** XRD patterns of BCTO ceramics prepared by the sol–gel method at different concentrations, **b** frequency dependence of the dielectric constant for BCTO ceramics prepared by the sol–gel at different concentrations and **c** dielectric constant at 1 kHz as a function of Ti concentration for BCTO ceramics

3 Results and discussion

3.1 Coagulating conditions

There are various parameters in the preparation of the precursor powders by the sol–gel process. Among these parameters, Ti concentration, reaction temperature, and aging time of the gel are particularly important for the resultant sol. Figure 1a presents the XRD patterns of BCTO ceramics at different Ti concentrations. As shown in Fig. 1a, the phase structure in all the ceramics is pure perovskite phase and no secondary phase is detected, which

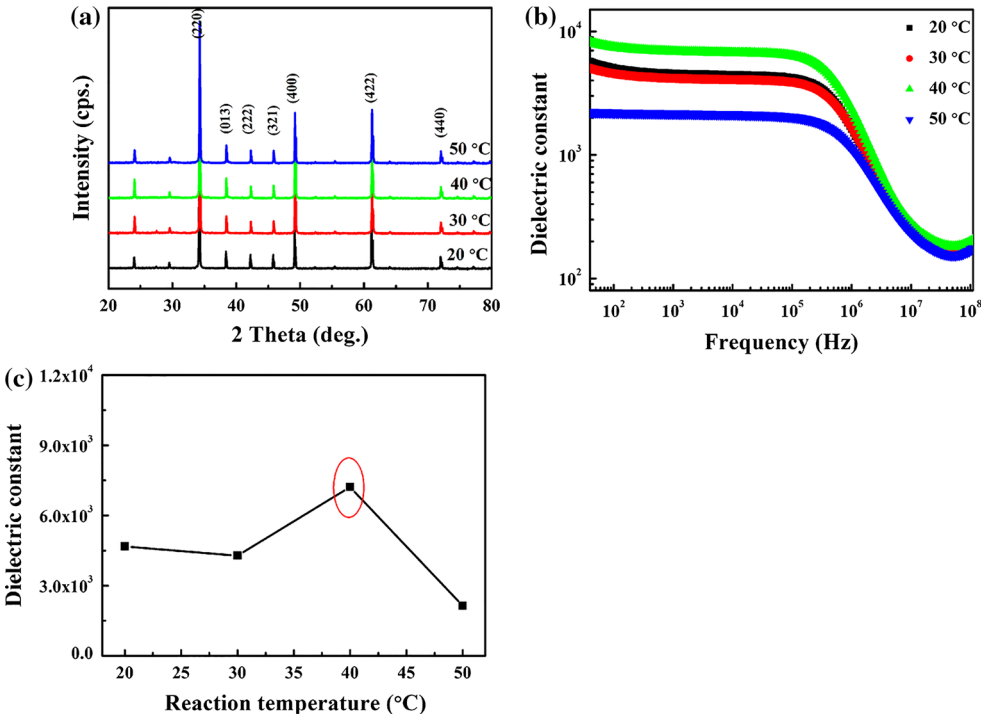

Fig. 2 **a** XRD patterns of BCTO ceramics prepared by the sol–gel method at different reaction temperatures, **b** frequency dependence of the dielectric constant for BCTO ceramics prepared by the sol–gel at different reaction temperatures and **c** dielectric constant at 1 kHz as a function of reaction temperature for BCTO ceramics

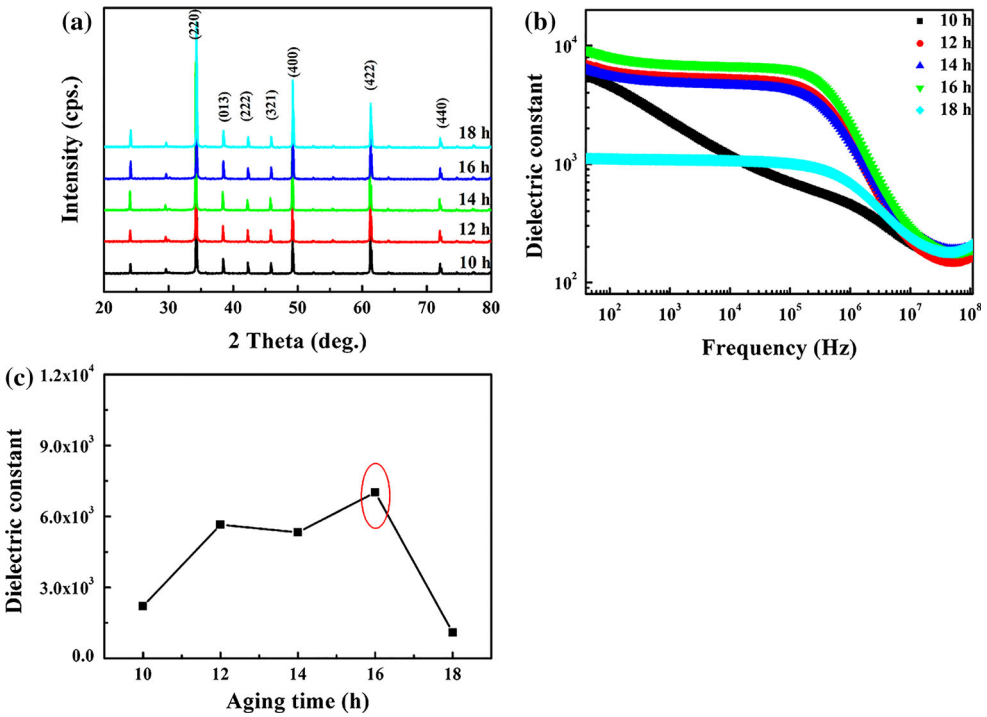

Fig. 3 **a** XRD patterns of BCTO ceramics prepared by the sol–gel method at different aging times, **b** frequency dependence of the dielectric constant for BCTO ceramics prepared by the sol–gel at different aging time and **c** dielectric constant at 1 kHz as a function of aging time for BCTO ceramics

corresponds to the standard diffraction pattern of CCTO (JCPDS card no: 75-2188) [12]. Figure 1b shows the frequency dependence of dielectric constant for BCTO ceramics with different Ti concentrations. All BCTO ceramics exhibit giant dielectric constant below 1 MHz. It can also be observed from Fig. 1b that the dielectric constant of BCTO ceramics increases with the increase of the Ti concentrations. The dielectric constant reaches the maximum value when the Ti concentration is 0.62 mol/L. Figure 1c shows dielectric constant at 1 kHz as a function of Ti concentration for BCTO ceramics. It is evident that the maximum dielectric constant value of 8,246 is achieved when the Ti concentration is 0.62 mol/L.

Figure 2a demonstrates the XRD patterns of BCTO ceramics at different reaction temperatures. It is found that the main crystalline phase is formed in all prepared ceramics and no any impurity is detected. Figure 2b presents the frequency dependence of dielectric constant for BCTO ceramics at different reaction temperatures. The dielectric constant of BCTO ceramics increases with the increase of the reaction temperatures, and reaches the maximum value when the reaction temperature is 40 °C. Figure 2c shows dielectric constant at 1 kHz as a function of reaction temperatures for BCTO ceramics. It can be found in Fig. 2c that the dielectric constant reaches the maximum value of 7,216 when the reaction temperature is 40 °C.

Figure 3a reveals the XRD patterns of BCTO ceramics obtained from the sol prepared at different aging times. The phase structure for all ceramics is pure perovskite phase and no any impurity is identified. Figure 3b shows the dielectric dispersion spectra for BCTO ceramics prepared at different aging times. From Fig. 3b, with increasing the aging time, the dielectric constant of the BCTO ceramics increases and reaches the maximum value when the aging time is 16 h. Figure 3c shows dielectric constant at 1 kHz as a function of reaction temperature for BCTO ceramics. From Fig. 3c, the maximum dielectric constant value of 7,037 is obtained when the aging time is 16 h.

It can be concluded that the Ti concentration, the reaction temperature and the aging time have significant effect on dielectric properties of the resultant ceramics. The optimum parameters for the preparation of BCTO precursor powders by the sol–gel method can be summarized as: the Ti concentration is 0.62 mol/L, the reaction temperature is 40 °C, and the aging time is 16 h.

3.2 Sintering conditions

Figure 4 presents the XRD patterns for BCTO ceramics at (a) different calcining temperatures and (b) different sintering temperatures. Main diffraction peaks in these XRD patterns can be indexed by a body centered cubic perovskite-related structure of space group *Im*3. With the increase of the calcining and sintering temperature, the intensities of the diffraction peaks corresponding to main crystal phase increase and reach the maximum when the calcining temperature is 800 °C and the sintering temperature is 1,000 °C, respectively.

Figure 5a–d show the SEM photographs on the surface of the ceramics calcined at different temperatures from 600 to 850 °C and sintered at 1,000 °C. As shown in Fig. 5a–d, the microstructures change significantly with the increase of the calcining temperature. With increasing the calcining temperature, the grain size firstly increases and then decreases. The porosity exhibits an opposite variation trend. When calcined at 800 °C, a relatively homogeneous microstructure with uniform size grain, clear grain boundaries, low porosity and compacted texture is obtained in Fig. 5c. However, the microstructure becomes inhomogeneous and abnormal grain growth is observed when the

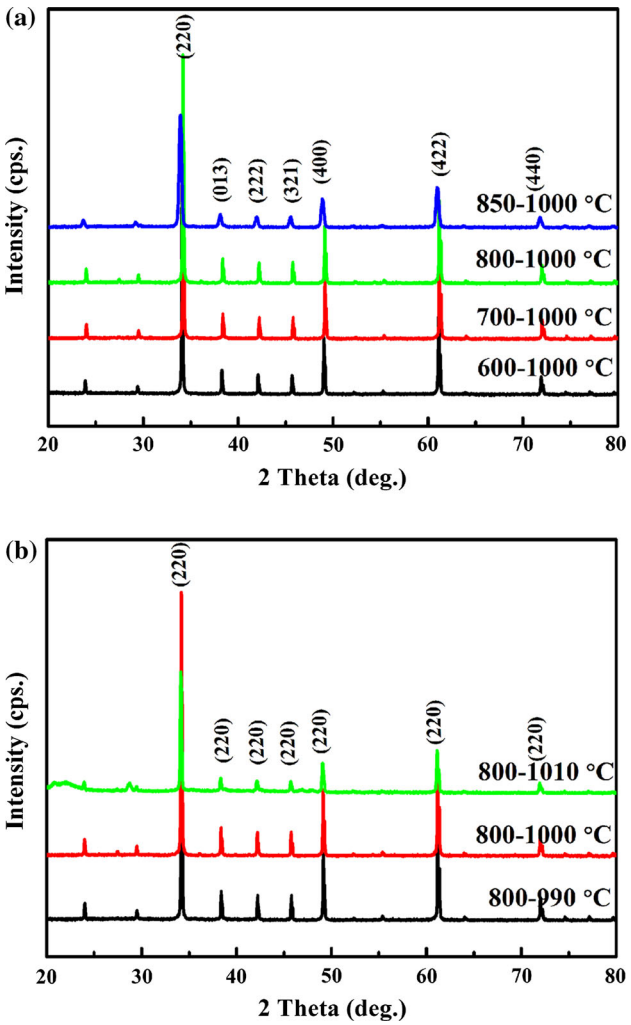

Fig. 4 **a** XRD patterns of BCTO ceramics at different calcining temperatures and **b** sintering temperatures

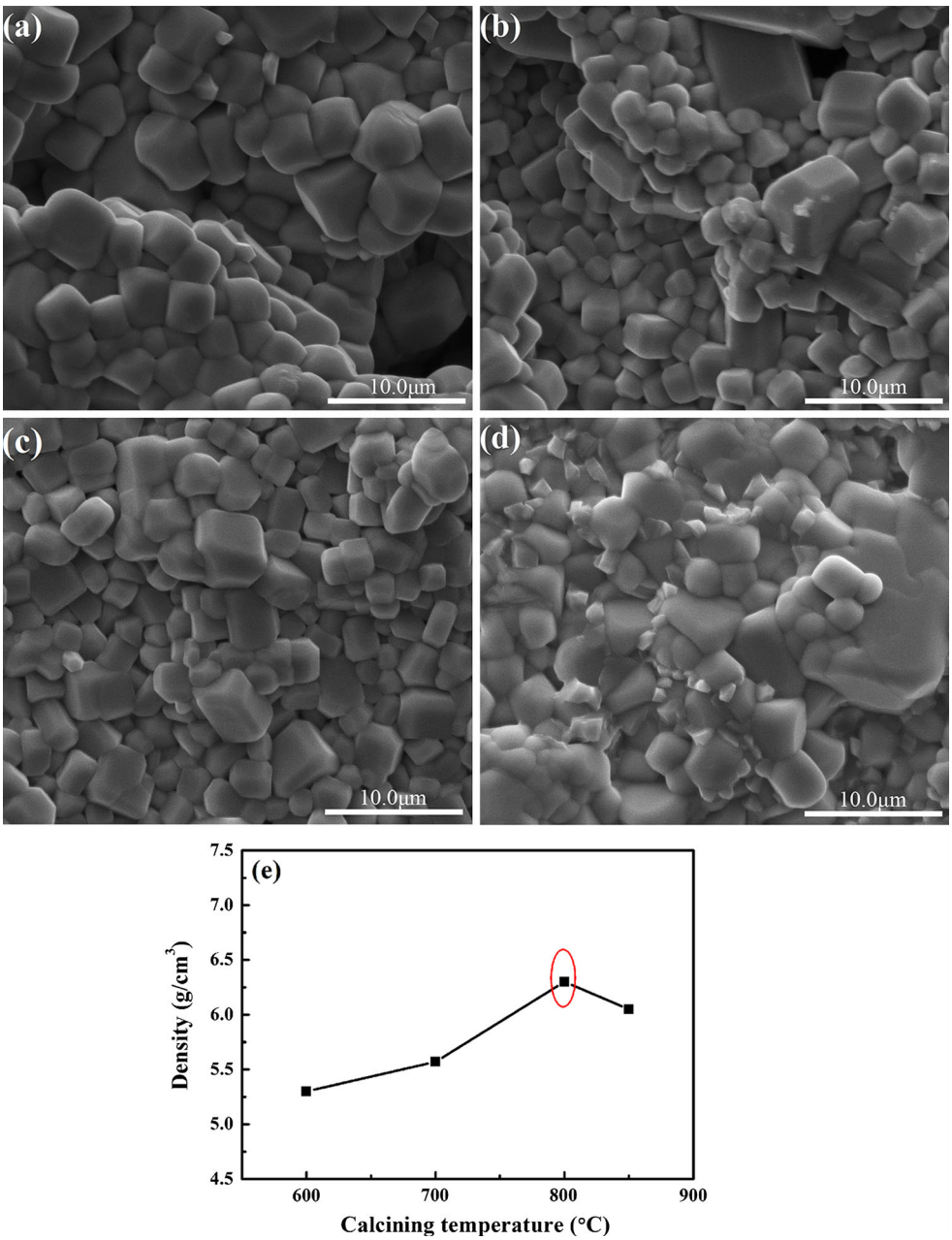

Fig. 5 SEM photographs on the surface of BCTO ceramics calcined at different temperatures from 600 to 850 °C, **a** 600 °C, **b** 700 °C, **c** 800 °C, **d** 850 °C and **e** densification behavior as a function of calcining temperature for BCTO ceramics

calcining temperature is 850 °C in Fig. 5d. This may be due to the existence of liquid phases formed during sintering process. Densification behavior as a function of calcining temperature for BCTO ceramics is presented in Fig. 5e. As shown in Fig. 5e, with increasing the calcining temperature, the density of BCTO ceramics calcined at 800 °C reaches the maximum value of 6.3 g/cm^3. Further increasing the calcining temperature causes a steep fall in the density, which is in agreement with the results of SEM photographs. The morphology and the density reveal that the optimum calcining temperature is 800 °C.

Figure 6a–c show the SEM photographs on the surface of the ceramics sintered at different temperatures from 990 to 1,010 °C. From Fig. 6a–c, the surface morphology of BCTO ceramics exhibit relatively homogeneous microstructure, clear grain boundaries. The surfaces of all samples show some differences, but the changes are not very noticeable. Compared to CCTO ceramics which are strongly dependent on processing conditions [9, 13–17], the surface morphologies of BCTO ceramics are nearly insusceptible to the sintering temperature. Figure 6d shows the densification behavior as a function of sintering

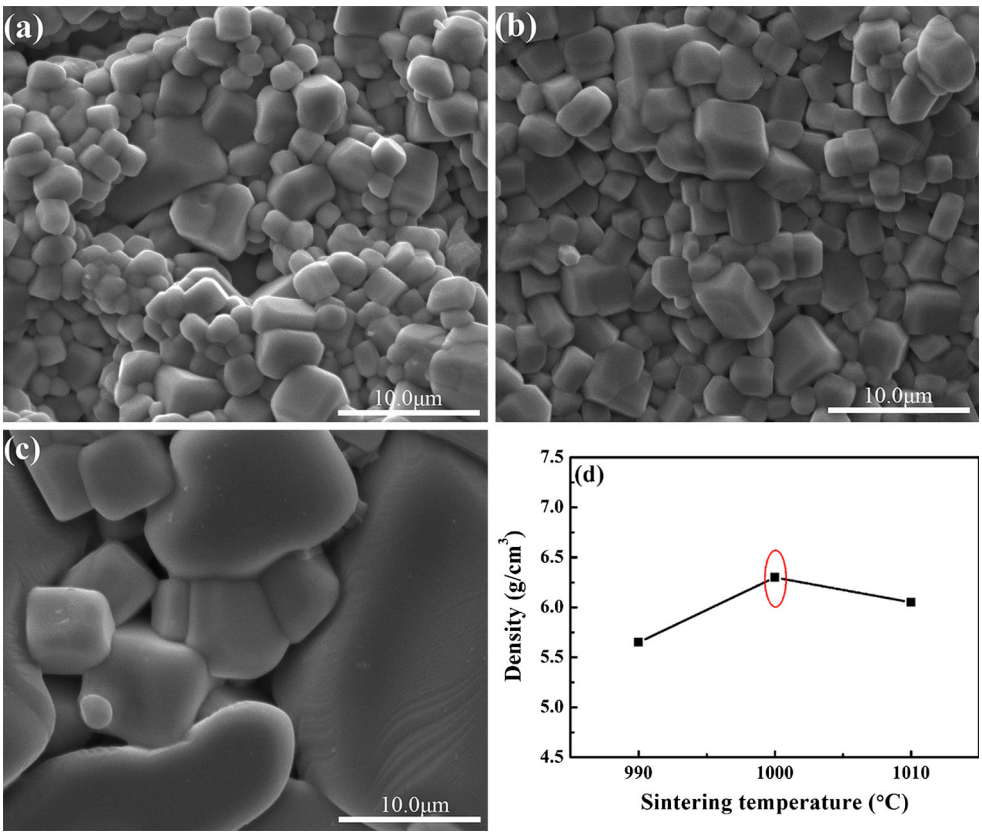

Fig. 6 SEM photographs on the surface of BCTO ceramics with different sintering temperatures, **a** 990 °C, **b** 1,000 °C, **c** 1,010 °C and **e** densification behavior as a function of sintering temperature for BCTO ceramics

temperature for BCTO ceramics. The density of BCTO ceramics increases with the increase of the sintering temperature. The maximum value of 6.3 g/cm^3 is achieved when sintered at 1,000 °C. Further increasing the sintering temperature causes a steep fall in the density, which is in agreement with the results obtained from Fig. 6a–c. Accordingly, the optimum sintering temperature is determined to be 1,000 °C.

Figure 7 demonstrates the frequency dependence of the dielectric constant and dielectric loss for BCTO samples prepared at different (a) calcining temperatures and (b) sintering temperatures. According to Fig. 7a, all samples exhibit giant dielectric constant and good frequency stability when the frequency is below 100 kHz. It is evident that the dielectric constant of BCTO ceramics increases and then gradually decreases with the increase of the calcining temperatures. The sample calcined at 800 °C exhibits the largest dielectric constant value of $\sim 1.2 \times 10^4$ at 1 kHz. When the measured frequency is over 100 kHz, the dielectric constant drops rapidly with further increasing frequency and then inclines almost to a constant, which can be explained by the Debye-type relaxation [11]. The giant dielectric constant may be attributed to Maxwell–Wagner effect occurring at the grain boundary [18]. It can be concluded that the improved dielectric properties could be optimized by varying the calcining temperatures. According to Fig. 7b, the sample sintered at 1,000 °C exhibit the largest low-frequency permittivity of $\sim 1.2 \times 10^4$ at 1 kHz. The results show that the dielectric constant of BCTO ceramics tends to increase significantly by changing the sintering temperature.

From all these results, the optimal dielectric properties of $\sim 1.2 \times 10^4$ at 1 kHz is obtained when the BCTO ceramics is calcined at 800 °C and sintered at 1,000 °C. Meanwhile, pure phase structure and the best microstructure are obtained as well.

3.3 Electric properties of BCTO ceramics prepared by different methods

Figure 8a shows the frequency dependence of the dielectric constant and dielectric loss for BCTO samples prepared by the sol–gel method (abbreviated as BCTO-SG samples) and by the solid-state reaction (abbreviated as BCTO-SS samples), respectively. Both BCTO-SG and BCTO-SS samples were prepared under the optimized processing parameters. From Fig. 8a, the frequency dependence of the dielectric constant for both samples display typical Debye-type relaxation feature. It can also be observed that the BCTO-SG samples exhibit outstanding giant dielectric constant (around 10,000) in the frequency range below 100 kHz, which is much higher than that of BCTO-SS

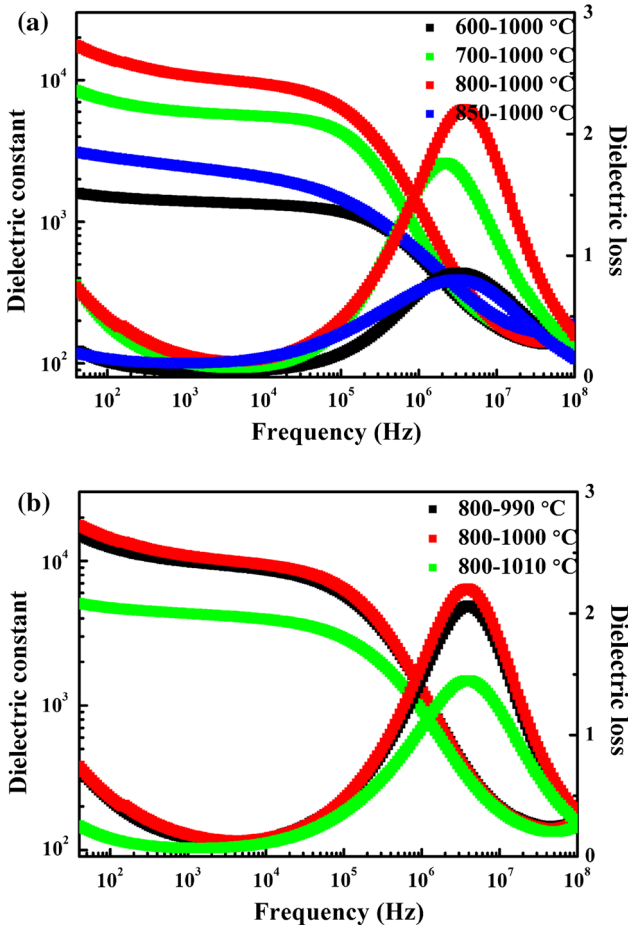

Fig. 7 Frequency dependence of the dielectric constant and loss at room temperature between 40 Hz and 110 MHz for BCTO ceramic samples prepared at different **a** calcining temperatures and **b** sintering temperatures

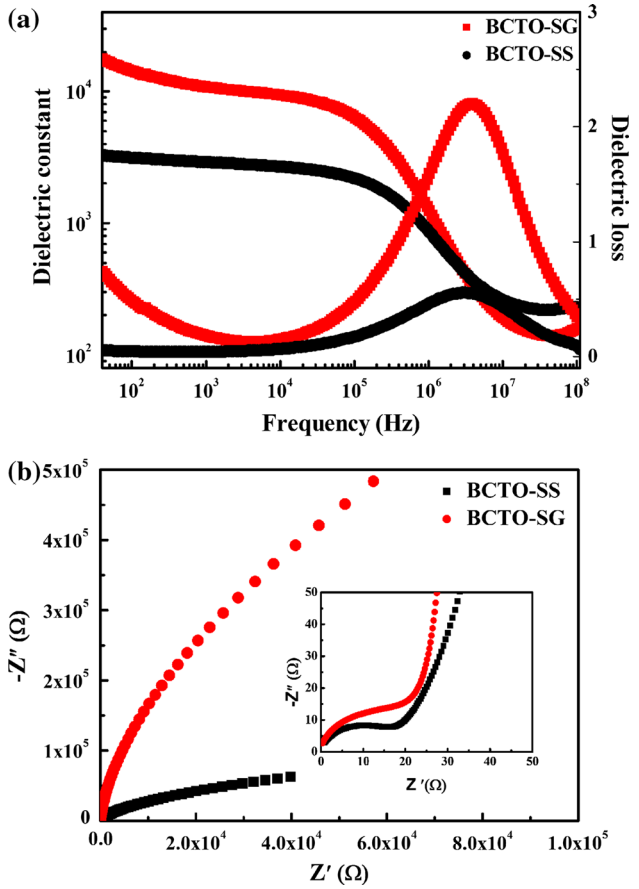

Fig. 8 **a** Frequency dependence of dielectric constant and loss of BCTO ceramics respectively prepared by the sol–gel and the solid-state reaction between 40 Hz and 110 MHz **b** complex impedance change of the BCTO ceramics prepared by the sol–gel method and prepared by the solid-state reaction

samples (~3,000 at 1 kHz). Furthermore, the dielectric constant of BCTO-SG samples is much higher than those reported in literature (1,750 and 1,871) [2, 8]. Figure 8b reveals the complex impedance of the BCTO-SG samples and BCTO-SS samples. The inset of Fig. 8b shows an expanded view of high-frequency data close to the origin. The curves of all the samples show a single semicircular arc with a nonzero high frequency intercept, indicating that all BCTO ceramics should be electrically heterogeneous. The higher frequency response corresponding to the small arc is associated with the grains, and the lower one is attributed to the grain boundaries. These two semicircular arcs can be modeled as an equivalent circuit consisting of two parallel *RC* elements connected in series: one *RC* element, i.e. R_gC_g, represents the semiconducting grains, and the other, i.e. $R_{gb}C_{gb}$, represents the insulating grain boundary regions. For such an equivalent circuit, each *RC* element ideally gives rise to semicircular arc in complex impedance plane Z* [19] described as follows:

$$Z^* = Z' - iZ'' \tag{1}$$

In AC circuits, for a pure resistor and capacitor, $Z^* = R$ and $1/i\omega C$, respectively. Therefore, the impedance can be expressed as Eq. (4) for each *RC* element.

$$Z^* = \frac{1}{1/R + i\omega C} = \frac{R}{1 + i\omega RC} \tag{2}$$

In our experiment, the impedance spectrum can be modeled as two *RC* elements connected in series. Therefore, the complex impedance here can be expressed as

$$Z' = \frac{R_g}{1 + \left(\omega R_g C_g\right)^2} + \frac{R_{gb}}{1 + \left(\omega R_{gb} C_{gb}\right)^2} \tag{3}$$

and

$$Z'' = R_g\left[\frac{\omega R_g C_g}{1 + (\omega R_g C_g)^2}\right] + R_{gb}\left[\frac{\omega R_{gb} C_{gb}}{1 + (\omega R_{gb} C_{gb})^2}\right] \tag{4}$$

where R and C are the resistance and capacitance, respectively, the subscripts g and gb refer to the grains and grain boundaries, respectively, and ω is the angular frequency. Based on Eq. (4), the response peaks of the grains and the grain boundaries are located at $1/(2\pi R_g C_g)$ and $1/(2\pi R_{gb} C_{gb})$, respectively, and the peak value is proportional to the associated resistance. The above results demonstrate that BCTO ceramics are electrically heterogeneous, which is well consistent with the internal barrier layer capacitance (IBLC) model [20–22]. The calculated grain boundary resistance and grain resistance of BCTO-SG samples were 0.59 MΩ and 23.69 Ω, and the corresponding values of BCTO-SS samples are 2.73 MΩ and 20.95 Ω, respectively. In general, the giant permittivity is mainly determined by the semiconducting grains based on IBLC effect, and the dielectric loss is closely related to the insulating grain boundaries. The higher the resistance of the grain is, the lower the low-frequency dielectric constant will be.

This result is further confirmed by the low temperature dependence of dielectric loss for BCTO ceramics. Figure 9 shows the low temperature dependence of dielectric loss for BCTO ceramics at 100, 300, 500 and 700 kHz (a) BCTO-SG samples and (b) BCTO-SS samples, respectively. A series of dielectric loss peaks are observed, which shift to higher temperature with the increase of measurement frequency. This indicates a thermal activation behavior. As shown in the insets of Fig. 9, a good linear relationship between ln (f_p) and $1/T$ is satisfied, and the variation relation obeys the Arrhenius law,

$$f_p = f_0(-E_a/k_B T) \tag{5}$$

where f_p is the peak frequency, f_o is the pre-exponential term, E_a is the activation energy, and K_B is the Boltzmann constant. The activation energies of the grain for BCTO-SG samples and BCTO-SS samples are 0.074 and 0.12 eV, respectively. The lower E_a value corresponds to the much higher giant dielectric constant [23]. In the present work, the E_a value of the BCTO-SG samples is lower than that of the BCTO-SS samples, leading to a larger dielectric constant, which is consistent with the results obtained from Fig. 8a.

Figure 10 demonstrates the temperature dependence of dielectric constant for BCTO ceramics at 1, 3, 5 and 7 kHz (a) BCTO-SG samples and (b) BCTO-SS samples, respectively. Figure 10a indicates that there exist two dielectric relaxations (indicated by the arrows and named as I and II respectively) in BCTO-SG samples. A careful examination reveals that the low-temperature dielectric relaxation occurred at ~200 °C in both samples (dielectric relaxation I) characterized by a broad peak. And the peak gets smaller and shifts to higher temperature as the

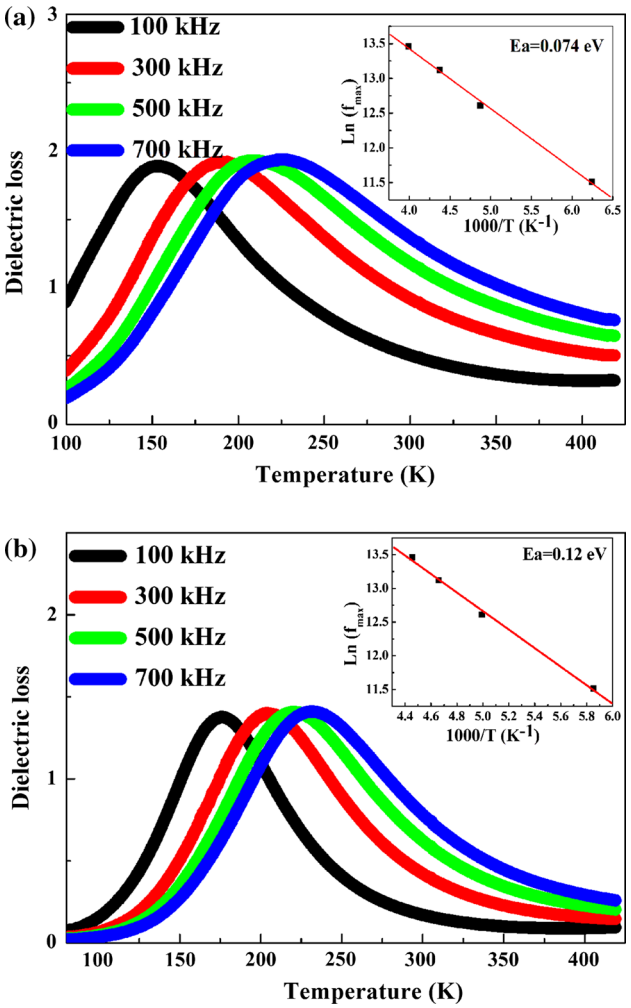

Fig. 9 Temperature (low temperature region) dependence of dielectric loss for BCTO ceramics at 100, 300, 500 and 700 kHz prepared by **a** the sol–gel method and **b** prepared by the solid-state reaction. The *inset* shows the Arrhenius plots for the two relaxations

measuring frequency increases, which suggests a thermally activated process. The literature [24] also confirmed that dielectric relaxation I was associated with Maxwell–Wagner relaxation. Interestingly, the low-temperature relaxation can only be observed in Fig. 10a, which exists at ~300 °C (dielectric relaxation II). It is almost frequency-independent and hardly changes its position, and the similar dielectric relaxation was reported in the literatures [25, 26]. These literatures lead us to suppose that the dielectric relaxation II may be concerned with the distribution state transition for oxygen vacancies.

To clarify the result further, the relaxation behavior of grain boundary is established. Figure 11 shows frequency dependence of Z'' for BCTO ceramics BCTO-SG samples (a) and BCTO-SG samples (b) (each step increase in measured temperature is 25 °C); inset shows Arrhenius plots for BCTO ceramics. As shown in Fig. 11, Z'' peaks

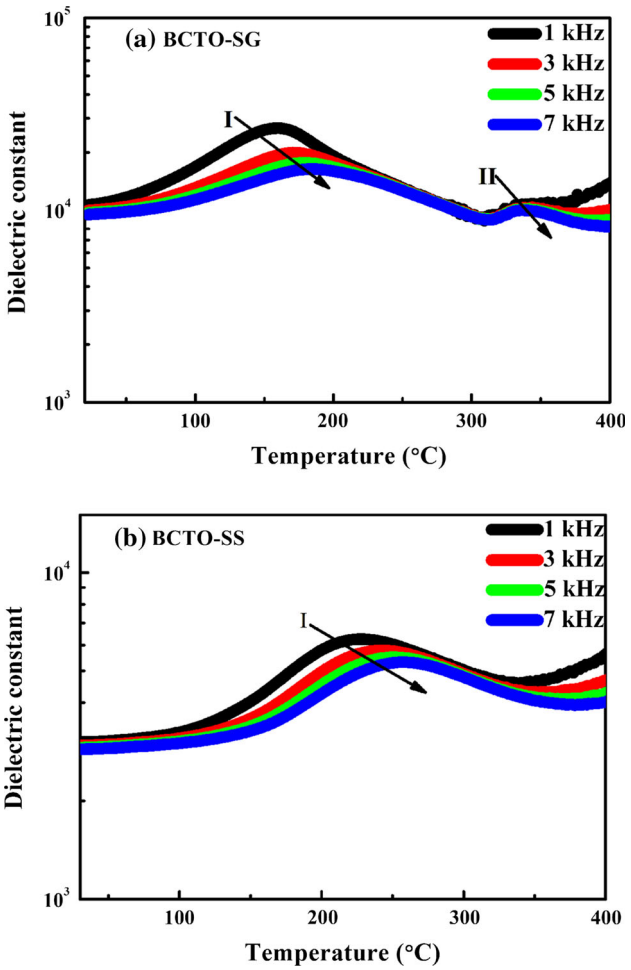

Fig. 10 Temperature dependence of dielectric constant for BCTO ceramics at 1, 3, 5 and 7 kHz prepared by **a** the sol–gel method and **b** prepared by the solid-state reaction

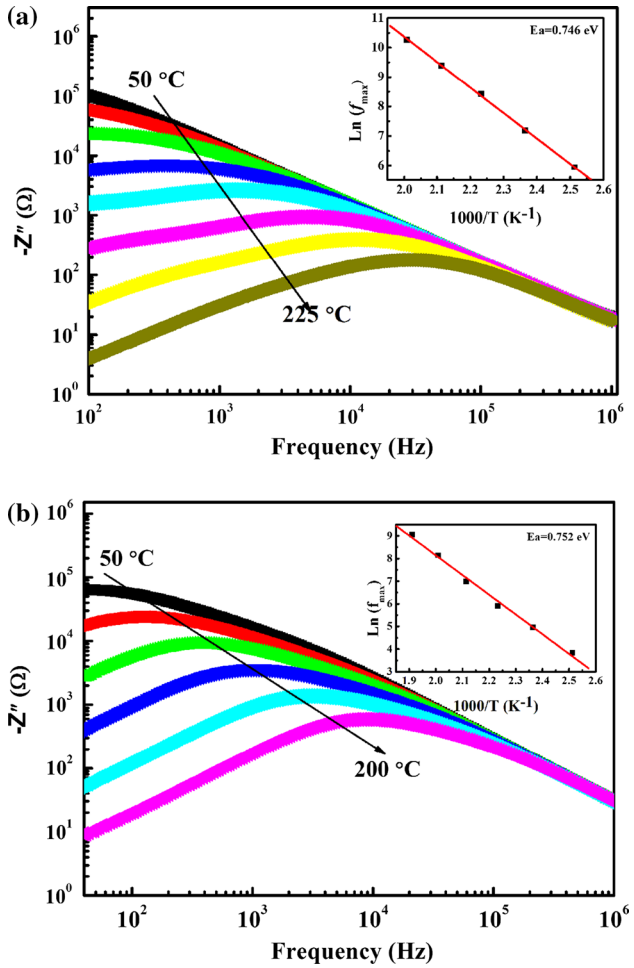

Fig. 11 Frequency dependence of Z'' for BCTO ceramics at the measuring temperature range prepared by **a** the sol–gel method **b** the solid-state reaction (each step increase in measured temperature is 25 °C)

shift to higher frequencies with the increase of the temperature, indicating a thermally activated response. In general, each element corresponds to the occurrence of one Debye-relaxation peak in Z'' (f) plots according to IBLC model. Therefore, the observed impedance peaks are ascribed to the grain boundary responses. The relation is described in the inset of Fig. 11, which obeys the Arrhenius law well [27]. The values of E_a for BCTO ceramics are calculated from the slopes of plots of ln$f$ versus 1,000/T. E_a value for BCTO-SG samples and BCTO-SS samples are found to be 0.746 and 0.752 eV, respectively. The two values are very close, which suggests that both samples may exhibit the same relaxation behavior in the measured temperature range. Similar results of the high-temperature dielectric relaxation in $Bi_{2/3}Cu_3Ti_4O_{12}$ (0.662 eV) [8], CCTO (0.720 eV) [28], and $La_{2/3}Cu_3Ti_4O_{12}$ (0.590 eV) [29] ceramics lead us to conclude that the dielectric relaxation I is concerned with the Maxwell–Wagner relaxation.

To confirm the result that the observed dielectric relaxation II is related to oxygen vacancies, we conduct dielectric measurements after a series of annealing treatments in O_2 atmospheres. Figure 12 presents the comparison of the dielectric behaviors for the as-sintered samples and the O_2-annealed samples, which shows some important information on the physical nature of the dielectric relaxation II. The dielectric relaxation II dielectric constant peak is significantly suppressed by O_2 annealing, indicating that the dielectric relaxation II is an extrinsic mechanism, and that the dielectric relaxation II is truly related to oxygen vacancies.

To sum up, the much higher low-frequency dielectric constant of BCTO-SG samples may be caused by two reasons. The first reason is that the sol–gel method has some advantages over the solid-state reaction. By the sol–gel method raw materials are likely to be mixed uniformly in the molecular level in a very short time, and the nano-

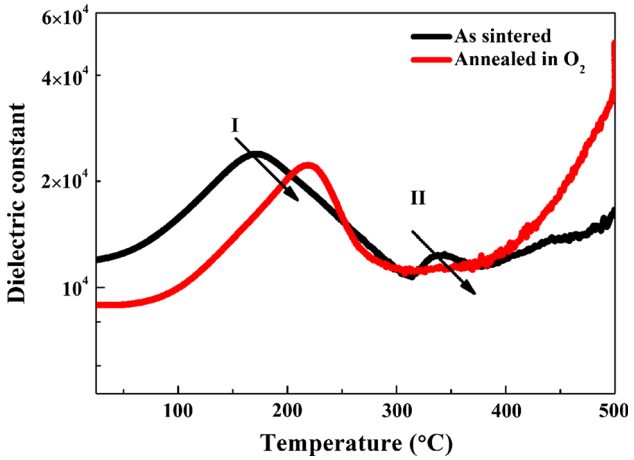

Fig. 12 Effects of annealing on temperature dependence of the dielectric constant of BCTO ceramics at 1 kHz. Annealing condition at 1,073 K in oxygen for 6 h

scale particle size lower reaction temperature which leads to the higher activity powders. The second reason is that the lower activation energy of grains for BCTO-SG samples corresponds to the higher dielectric constant. In short, the sol–gel method is an effective way to improve the electrical properties of BCTO ceramics.

4 Conclusion

Nominally pure BCTO ceramics were synthesized via the sol–gel method. When the Ti concentration was 0.62 mol/L, the aging time was 16 h, the reaction temperature was 40 °C, the calcining temperature was 800 °C, and the sintering temperature was 1,000 °C, BCTO ceramics gained the excellent dielectric properties with a dielectric constant of $\sim 1.2 \times 10^4$ (at 1 kHz). Obviously, the dielectric constant of the BCTO-SG samples was much higher than that of BCTO-SS samples ($\sim 0.30 \times 10^4$). The complex impedance analysis indicated that both two BCTO ceramics were electrically heterogeneous, consisting of insulating grain boundaries and semiconducting grains, which was well consistent with the IBLC model. According to IBLC effect, the lower activation energy of grains for BCTO-SG samples contributed to a higher low-frequency dielectric constant of BCTO-SG samples. In addition, dielectric relaxation I occurred at ~200 °C for BCTO ceramics irrespective of the preparation method was ascribed to the Maxwell–Wagner relaxation. The dielectric relaxation II only observed in the temperature dependence of dielectric constant at ~300 °C for BCTO-SG samples was attributed to the variation on oxygen vacancies state, since it could be suppressed by O_2-annealing.

Acknowledgments This work was supported by National Science Foundation of China (NSFC) (Grant Nos. 51172136 and 51107077) and the Fundamental Research Funds for the Central Universities (Program Nos. GK201101003, GK201101004, GK201301002, GK201305013 and GK201403006) and Science and Technology Program of Shaanxi Province and Xi'an City (Grant Nos. 2013K09-26 and CXY1342(4)).

References

1. M.A. Subramanian, D. Li, N. Duan, B.A. Reisner, A.W. Sleight, J. Solid State Chem. **151**, 323 (2000)
2. M.A. Subramanian, A.W. Sleight, Solid State Sci. **4**, 347 (2002)
3. J.J. Liu, C.G. Duan, W.N. Mei, R.W. Smith, J.R. Hardy, J. Appl. Phys. **98**, 093703 (2005)
4. M.C. Ferrarelli, T.B. Adams, A. Feteira, D.C. Sinclair, A.R. West, Appl. Phys. Lett. **89**, 212904 (2006)
5. R.Q. Zuo, L.X. Feng, Y.Y. Yan, B. Chen, G.H. Cao, Solid State Commun. **138**, 91 (2006)
6. D. Szwagierczak, J. Electroceram. **23**, 56 (2008)
7. W.T. Hao, J.L. Zhang, Y.Q. Tan, W.B. Su, J. Am. Ceram. Soc. **92**, 2937 (2009)
8. J.J. Liu, C.G. Duan, W.G. Yin, W. Mei, R. Smith, J. Hardy, Phys. Rev. B **70**, 144106 (2004)
9. L.J. Liu, H.Q. Fan, P.Y. Fang, X.L. Chen, Mater. Res. Bull. **43**, 1800 (2008)
10. B. Xu, J. Zhang, Z. Tian, S.L. Yuan, Mater. Lett. **75**, 87 (2012)
11. Z.Q. Liu, G.S. Jiao, X.L. Chao, Z.P. Yang, Mater. Res. Bull. **48**, 4877 (2013)
12. W.Q. Ni, X.H. Zheng, J.C. Yu, J. Mater. Sci. **42**, 1037 (2007)
13. T.B. Adams, D.C. Sinclair, A.R. West, Adv. Mater. **14**, 1321 (2002)
14. T.T. Fang, H.K. Shiau, J. Am. Ceram. Soc. **87**, 2072 (2004)
15. B.A. Bender, M.J. Pan, Mater. Sci. Eng. B **117**, 339 (2005)
16. J.L. Zhang, P. Zheng, C.L. Wang, M.L. Zhao, J.C. Li, J.F. Wang, Appl. Phys. Lett. **87**, 142901 (2005)
17. S.F. Shao, J.L. Zhang, P. Zheng, W.L. Zhong, C.L. Wang, J. Appl. Phys. **99**, 084106 (2006)
18. P.B. Shri, K.B.R. Varma, Phys. B **403**, 2246 (2008)
19. D.C. Sinclair, T.B. Adams, F.D. Morrison, A.R. West, Appl. Phys. Lett. **80**, 2153 (2002)
20. J. Li, A.W. Sleight, M.A. Subramanian, Solid State Commun. **135**, 260 (2005)
21. Z.P. Yang, L.J. Zhang, X.L. Chao, L.R. Xiong, J. Liu, J. Alloy. Compd. **509**, 8716 (2011)
22. H.M. Ren, P.F. Liang, Z.P. Yang, Mater. Res. Bull. **45**, 1608 (2010)
23. P.F. Liang, Y.Y. Li, F.C. Li, X.L. Chao, Z.P. Yang, Mater. Res. Bull. **52**, 42 (2014)
24. B.S. Prakash, K.B.R. Varma, J. Phys. Chem. Solids **68**, 490 (2007)
25. L.N. Liu, C.C. Wang, C.M. Lei, T. Li, G.J. Wang, X.H. Sun, J. Wang, S.G. Huang, Y.D. Li, H. Wang, Appl. Phys. Lett. **102**, 112907 (2013)
26. C.C. Wang, C.M. Lei, G.J. Wang, X.H. Sun, T. Li, S.G. Huang, H. Wang, Y.D. Li, J. Appl. Phys. **113**, 094103 (2013)
27. Y.H. Lin, J.N. Cai, M. Li, C.W. Nan, J.L. He, J. Appl. Phys. **103**, 074111 (2008)
28. T. Adams, D. Sinclair, A. West, Phys. Rev. B **73**, 094124 (2006)
29. B.S. Prakash, K.B.R. Varma, J. Mater. Sci. Mater. Electron. **17**, 899 (2006)